Journal of Engineering Technology and Applied Sciences, 2025 *e-ISSN:* 2548-0391
Received 13 December 2023, Accepted 19 May 2025 *Vol. 10, No. 2, 97-113*
Published online 30 August 2025, Research Article *doi: 10.30931/jetas.1404278*

Citation: Alisoy, H., Mutlu, R., Korkmaz Tan, R., Çanta, H., "Evaluation of the Electric Field of a Single-Core Power Cable at the Inner Conductor Radius". Journal of Engineering Technology and Applied Sciences 10 (2) 2025 : 97-113.

EVALUATION OF THE ELECTRIC FIELD OF A SINGLE-CORE POWER CABLE AT THE INNER CONDUCTOR RADIUS

Hafiz Alisoy [a], Reşat Mutlu [a], Rabia Korkmaz Tan [b*], Hakan Çanta [c]

[a] Tekirdağ Namık Kemal Üniversitesi, Tekirdağ, Turkiye*
halisoy@nku.edu.tr, rmutlu@nku.edu.tr

[b] Tekirdağ Namık Kemal Üniversitesi, Çorlu Mühendislik Fakültesi, Bilgisayar Mühendisliği Bölümü Tekirdağ, Turkiye*
*rkorkmaz@nku.edu.tr (*corresponding author)*

[c] Unika Cable, Çerkezköy, Tekirdağ, Turkiye
hakan@unika.com.tr

Abstract

Dielectric strength is a very important parameter for cables. It can vary according to temperature and frequency. The complex electrical permittivity of the Cross-linked polyethylene (XLPE) and Copper Polyester/Mylar band layers of a cable determine the maximum electric field created inside the cable operating at sinusoidal voltage. The value of this electric field should be less than the dielectric strength of the materials used. The electrical characteristics of XLPE and Copper Polyester tape depend on frequency and temperature. In a power cable, the temperature depends on the radial position, which makes it difficult to calculate the cable's electric field. In this study, it was shown how to calculate the electric field of the cable by using XLPE and Copper Polyester band data taken from the literature and numerical integration. It was found that the calculated value is less than the Dielectric strength value of XLPE material. It has been shown how the electric field of the power cable under investigation changes according to frequency and temperature.

Keywords: Cable modeling, Single-core power cable, Cable dielectric strength, XLPE material

1. Introduction

Single-core power cables are widely used for power transmission [1]. Typically, XLPE and Mylar serve as insulation materials within these cables, with cable characteristics like complex permittivity and aging significantly influenced by temperature variations [1, 2]. Due to the importance of XLPE material, its characteristics such as leakage current, water treeing, and contact angle are examined for its better usage [3, 4]. Modeling cables presents a considerable challenge due to their inherent complexity [5]. The dielectric strength stands as a crucial safety parameter for insulators [6]. It's known to vary based on factors like frequency, temperature, and the material's thickness [7]. Upon experiencing a breakdown, a cable becomes inoperable, failing to meet the expected operational standards [8]. The maximum electric field specified by the operation voltage in a cable should stay below the dielectric strength [9]. Sometimes a safety factor can also be used for this purpose since an overvoltage also contributes to the aging of medium voltage XLPE Power Cables [10]. The dielectric strength of a material can also change with the humidity [11]. Isolation tests are conducted on electrical machinery and cables to assess their suitability for operation under specified conditions [10]. For a cable to operate without failure, the maximum electric field occurring within it should be calculated and its value should be less than the dielectric strength of the material used to minimize the time and expenses needed for the tests [12]. High-voltage technique literature often calculates the maximum electric field by modeling materials using a constant permittivity [12]. However, the assumption of constant permittivity does not hold true due to the temperature and frequency-dependent nature of materials [13, 14]. The complex relative permittivity of an XLPE sample is measured and presented as a function of temperature and frequency [15]. The experiments in [15, 16], employ a rectangular prism sample of XLPE. However, XLPE within a single-core power cable possesses a cylindrical geometry, requiring the calculation of its electric field to account for this shape. Furthermore, these cables encompass various components like Mylar, Armour, and Halogen Free Flame Retardant (HFFR) impacting their overall thermal behavior [17-19]. These regions make the calculation of the electric field of a single-core power cable more difficult. The harmonics created by the nonlinear loads can also contribute to the electric field within a cable and results in its additional heating [20]. Excessive heat and voltage stress can lead to premature aging of cables [21]. The type of operation voltage, AC or DC, also affects the breakdown voltage of the insulation materials [22]. To the best of our knowledge, the electrical field of a cable is calculated using a constant permeability in literature, not taking into account its operation frequency and the temperature distribution within the cable. That's why it is imperative and useful to have a method which gives the electric field within the different regions of a cable as a function of frequency and temperature by considering different cable insulator layers. In this study, the maximum electric field of an unaged single-core power cable is calculated by considering the frequency and temperature dependencies of the XLPE and Mylar materials, using numerical integration in the cylindrical coordinates, developing the necessary code in Matlab in steady-state, and comparing the calculated value with the dielectric strength of the materials to see whether the breakdown would occur or not. This algorithm can be used for designing single-core power cables and assessing their dielectric strength. In this study, the XLPE data is taken from [15], the Mylar data is taken from [23], the dielectric strength of XLPE is taken from [24], and the dielectric strength of Mylar materials is taken from [23], and the heat transfer parameter are taken from [21, 23-25].

The paper is arranged as follows. The second section introduces the heat transfer model for the single-core cable. The third section details the electrical permittivity models employed for the XLPE and Mylar insulators. In the fourth section, the maximum electric field values of the

power cable within the XLPE and Mylar layers are calculated using the established permittivity models. The paper is concluded with the conclusion section.

2. The thermal circuit of the single-core cable

A mathematical model of a cable line with cross-linked polyethylene insulation shown in Figure 1.a is made in this section. The cross-section of the cable is presented in Figure 1.b. The steady-state thermal circuit model of the single-core cable is given in Figure 2. When modeling the thermal circuit, the following assumptions are adopted:
— the cable has an ideal cylindrical shape;
— the parameters of the cable and its environment do not change along the axis.
Under these assumptions, the heat is uniformly distributed from the cable axis to its surface and dissipated from the surface into the environment.

In the equivalent circuit of the single-core cable, each layer (Figure 1.b) of the cable cross-section is represented in the form of thermal resistances (Figure 2). The thermal resistance of each cable layer is calculated using the radii of the concerned layer. The symbols of the radii are presented in Table 1. The thermal resistances of the cable depend on the material and the inner and outer radii of the cable layer.

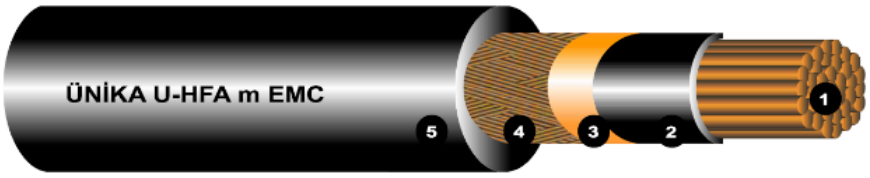

MAKE UP

1.	Conductor	:	Annealed Bare or Tinned stranded copper in accordance with IEC 60228 CL2 or CL5
2.	Insulation	:	Cross-linked polyethylene XLPE in accordance with IEC 60092-360
3.	Tape	:	Copper polyester tape
4.	Armour	:	Bare or Tinned copper wire braid in accordance with IEC 60092-350
5.	Outer Jacket	:	Halogen free extruded compound, SHF1 or SHF2 in accordance with IEC 60092-360

(a)

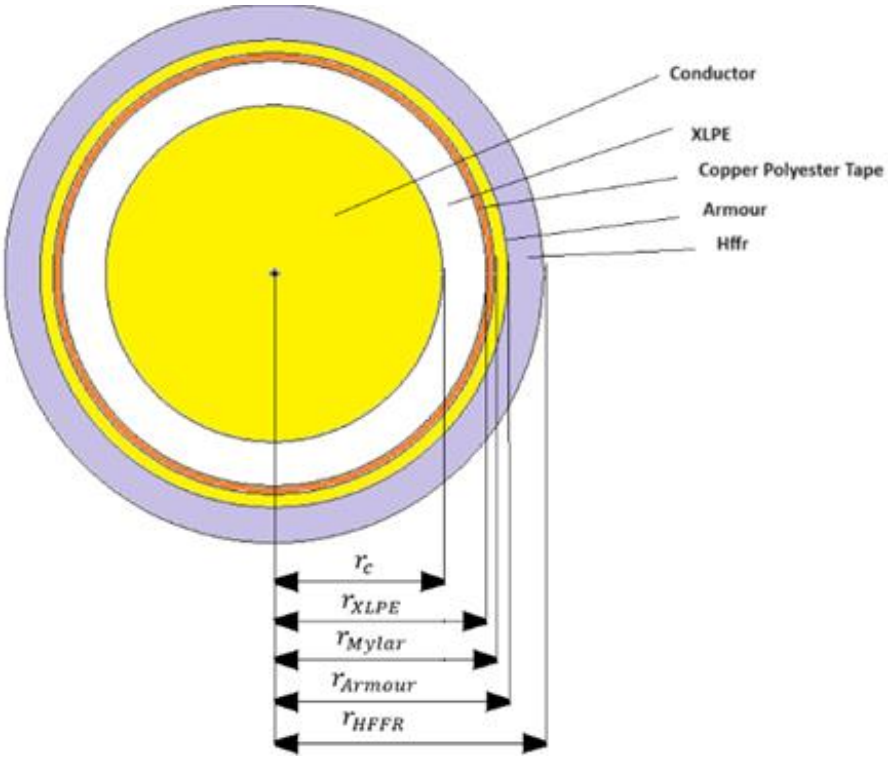

(b)

Figure 1. The side view of the single-core cable structure (Courtesy of UNİKA).

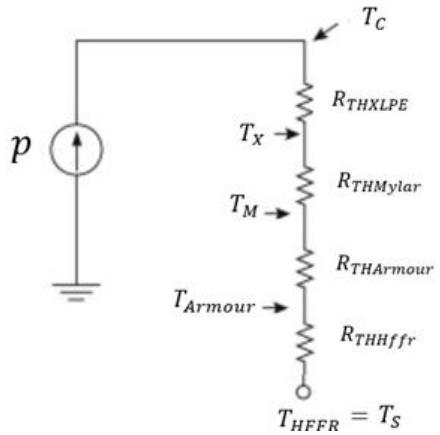

Figure 2. The steady-state thermal circuit of the single-core cable.

According to Joule-Lenz's law, the power loss within the copper conductor is calculated as

$$p = R_{AC} I_{rms}^2. \tag{1}$$

where I_{rms} is the effective current of the power cable, and R_{AC} is the AC resistance at the operation frequency.

Ignoring the end effects, the thermal resistance of a long hollow cylindric layer [26] is calculated as

$$R_{TH} = \frac{ln(r_{out}/r_{in})}{2\pi kL}. \tag{2}$$

where L, r_{in}, and r_{out} are, respectively, the length, the inner radius, and the outer radius of the layer, and k is its thermal conductivity.

The radii of the layers of the examined single-core cable are given in Table 1. The thermal conductivity of each layer is given in Table 2. The heat conductivities of Copper and the HFFR compound are adapted from [21]. The heat conductivity of Mylar is adapted from [21]. The heat conductivity of XLPE is adapted from [25]. The conductor temperature should not exceed 90 °C [19]. The ambient and conductor temperatures are used as 20 °C and 90 °C, respectively, in the calculations as done in [28]. For a long single-core cable, the formulas and the calculated values of the thermal resistance of the layers are given in Table 3.

Table 1. The radii of the layers of the single-core cable [28].

Name	Symbol	Value (mm)
The Copper wire radius	r_c	7.62
The XLPE layer outer radius	r_{XLPE}	9.62
The Mylar layer outer radius	r_{Mylar}	9.99
The Armour layer outer radius	r_{Armour}	10.59
The HFFR layer outer radius	r_{HFFR}	12.19

Table 2. The thermal conductivities of the cable layers [28].

Material	Thermal Conductivity Symbol	Thermal Conductivity Value ($W \cdot m^{-1} \cdot K^{-1}$)
Copper	$k_{Armour} = k_{Copper}$	398
XLPE	k_{XLPE}	0.28
Mylar	k_{Mylar}	0.155 (At the temperature range of 25.0 - 75.0 °C)
HFFR	k_{HFFR}	0.25

Table 3. The thermal resistance of the layers.

The layer name	Thermal resistance of the layer	Its value (W/K)
XLPE	$R_{THXLPE} = \frac{ln(r_{XLPE}/r_c)}{2\pi k_{XLPE} L}$	0.1324
Mylar	$R_{THMylar} = \frac{ln(r_{Mylar}/r_{XLPE})}{2\pi k_{Mylar} L}$	0.03875
Armour	$R_{THArmour} = \frac{ln(r_{Armour}/r_{Mylar})}{2\pi k_{Armour} L}$	2.411e-5
HFFR	$R_{THHffr} = \frac{ln(r_{Hffr}/r_{Armour})}{2\pi k_{Hffr} L}$	0.07837

Using the thermal circuit analogy, in the steady state, the temperature distributions needed are found as follows. In the steady state, the XLPE temperature (T_X) at $r = r_{XLPE}$ is found as

$$T_X = T_C - \frac{R_{THXLPE}(T_C - T_S)}{R_{THXLPE} + R_{THMylar} + R_{THArmour} + R_{THHffr}}. \quad (3)$$

The simulations are done with the thermal conductivity values presented in Table 2. The temperature in the XLPE insulator is calculated as

$$T(r) = (T_C - T_X)\frac{\ln(r/r_{XLPE})}{\ln(r_C/r_{XLPE})} + T_X. \quad (4)$$

In the steady state, the Mylar temperature (T_M) at $r = r_{Mylar}$ is calculated as

$$T_M = T_X - \frac{R_{THMylar}(T_X - T_M)}{R_{THXLPE} + R_{THMylar} + R_{THArmour} + R_{THHffr}}. \quad (5)$$

The temperature in the Mylar layer is calculated as

$$T(r) = (T_X - T_M)\frac{\ln(r/r_{Mylar})}{\ln(r_{XLPE}/r_{Mylar})} + T_M. \quad (6)$$

The steady-state heat transfer analysis of the cable is made using Equations (3)-(6) and the calculated temperatures at the layer boundaries are presented in Table 4 as similarly done in [28]. The temperatures with respect to the radial position within the XLPE and Mylar insulators are illustrated in Figure 3. They are used to calculate the maximum electric field occurring on the inner conductor by also taking the operation frequency into account.

Table 4. The temperatures at the interface boundaries.

The temperature	**Its value**
The conductor temperature at $r = r_C$, T_C	90 ^{0}C
The XLPE temperature at $r = r_{XLPE}$, T_X	55.50 ^{0}C
The copper polyester (Mylar) band temperature at $r = r_{Mylar}$, T_M	45.41 ^{0}C
The copper armour temperature at $r = r_{Armour}$, T_{Armour}	45.40 ^{0}C
The ambient temperature or the HFFR temperature at $r = r_{HFFR}$, $T_{HFFR}(= T_S)$	25 ^{0}C

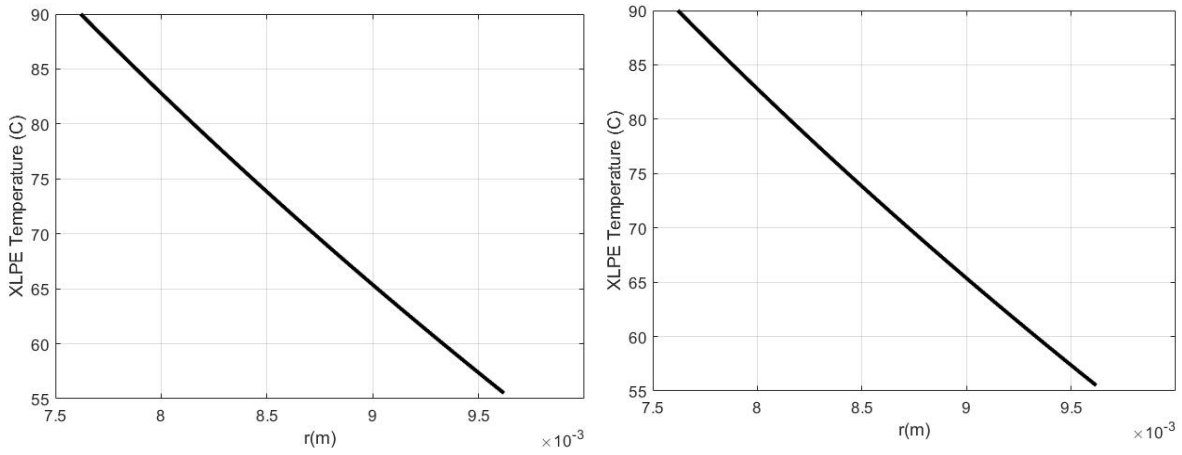

(a) (b)

Figure 3. The temperature within a) the XLPE and b) the Mylar vs. radial distance.

3. Complex permittivity model of the insulators

In this section, the electrical permittivity models of the insulator materials used in the power cable are presented as done in a similar way in [28].

3.1 Complex permittivity model of the XLPE insulator

In this subsection, the relative complex permittivity components of the XLPE layer of the power cable are presented. The complex permittivity of the XLPE material is measured and given in [15], In this paper, the data given in [15] is reproduced with Getdata program [27]. The leakage impedance of the cable is calculated using the reproduced data from [15] in [28]. Also, ANN models of the data can be found in [29]. Both the real and complex parts of the permittivity are assumed to be a function of temperature (*T*) and frequency (*f*). They are illustrated in Figures 4 and 5, respectively. The complex permittivity of the XLPE material is expressed as

$$\varepsilon_{\mathrm{XLPE}}(f,T) = \varepsilon_0 \varepsilon'(f,T) - j\varepsilon_0 \varepsilon''(f,T). \quad (7)$$

where $\varepsilon'$and $\varepsilon''$is the real and imaginary components of the relative complex permittivity, and $\varepsilon_0 = 8.85 \cdot 10^{-12}$ F/m is the permittivity of vacuum.

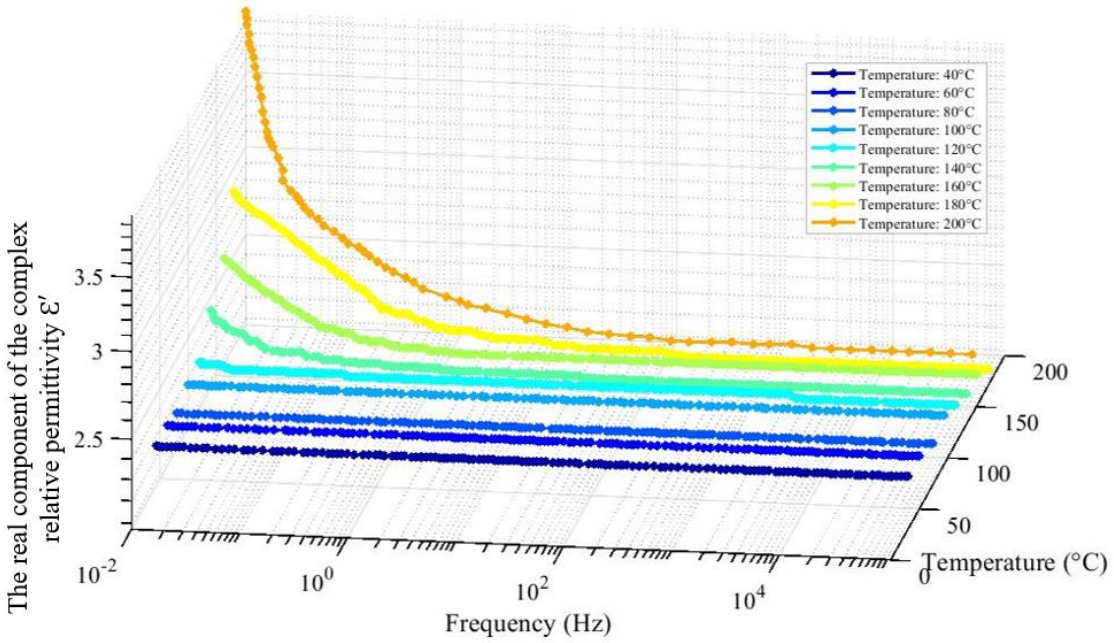

Figure 4. The reproduced real component of the complex relative permittivity ε' of the XLPE material measured as a function of frequency and temperature in [15].

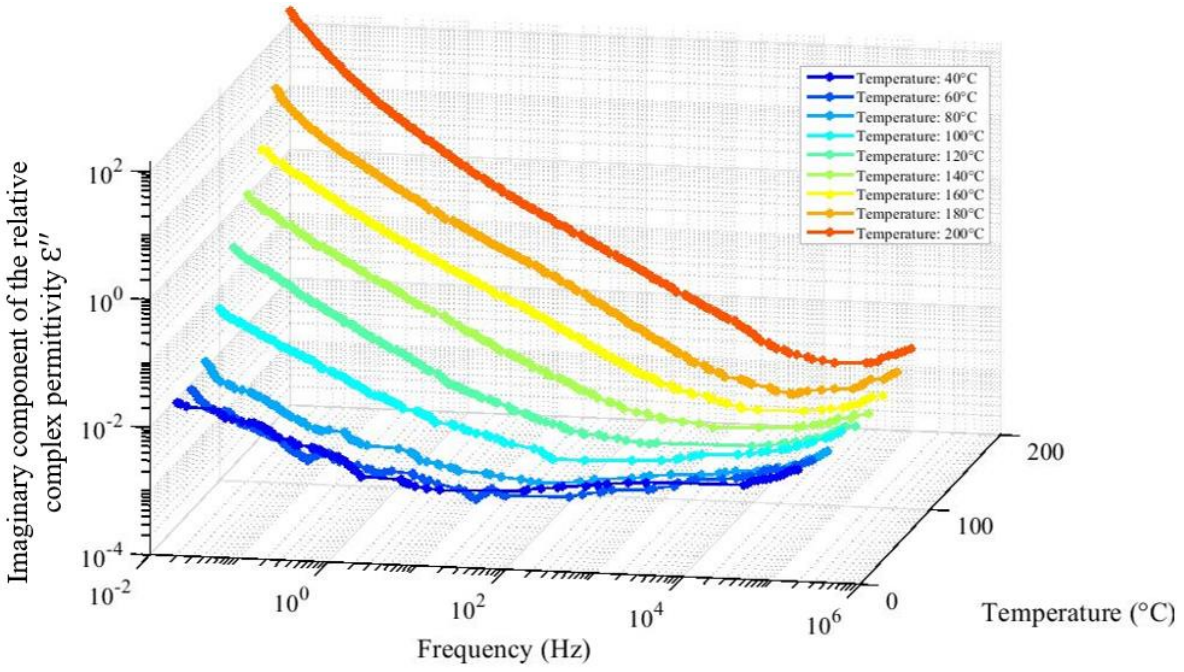

Figure 5. The reproduced imaginary component of the complex relative permittivity ε'' of the XLPE material measured as a function of frequency and temperature in [15].

3.2 Complex Permittivity Model of the Mylar Insulator

In this subsection, the relative permittivity and dissipation factor of Mylar insulator are presented. The electrical properties of Mylar given in [23] are reproduced with Getdata program [27]. The data retrieved from [23] was less extensive than the XLPE data acquired from [15].

The relative permittivity, $\varepsilon_{\text{Mylar}}(f,T)$, and the dissipation factor, $DP_{\text{Mylar}}(f,T)$, of Mylar are assumed to be functions of temperature (T) and frequency (f) as done in [28]. They are illustrated in Figures 6 and 7, respectively. The electrical conductivity of Mylar insulator is found as

$$\sigma_{\textbf{Mylar}}(f,T) = \omega\varepsilon_0\varepsilon_{\textbf{Mylar}}(f,T)DP_{\textbf{Mylar}}(f,T), \tag{8}$$

where $\omega = 2\pi f$ is the angular frequency.

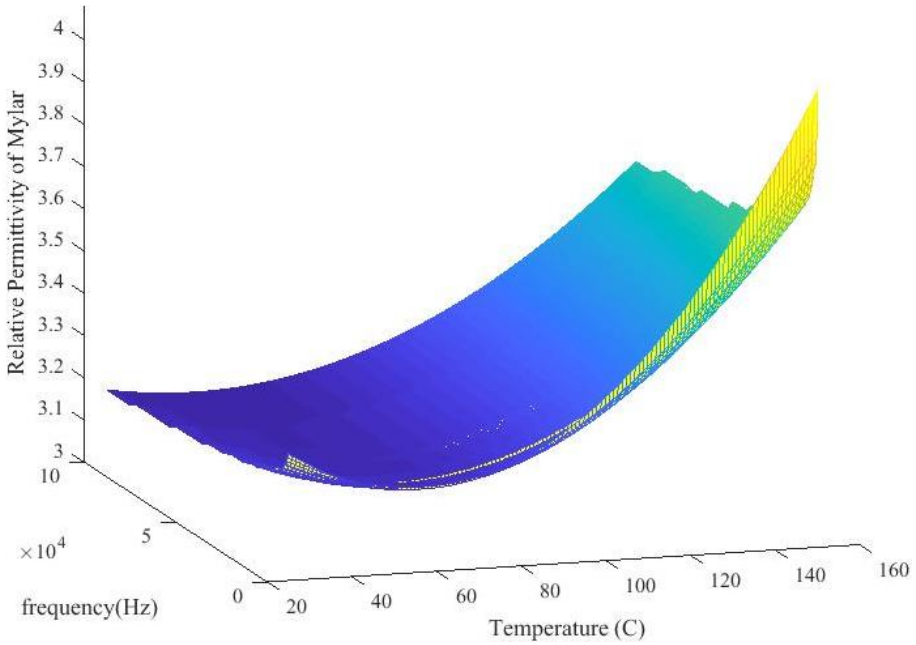

Figure 6. The relative permittivity of the Mylar vs. temperature and frequency.

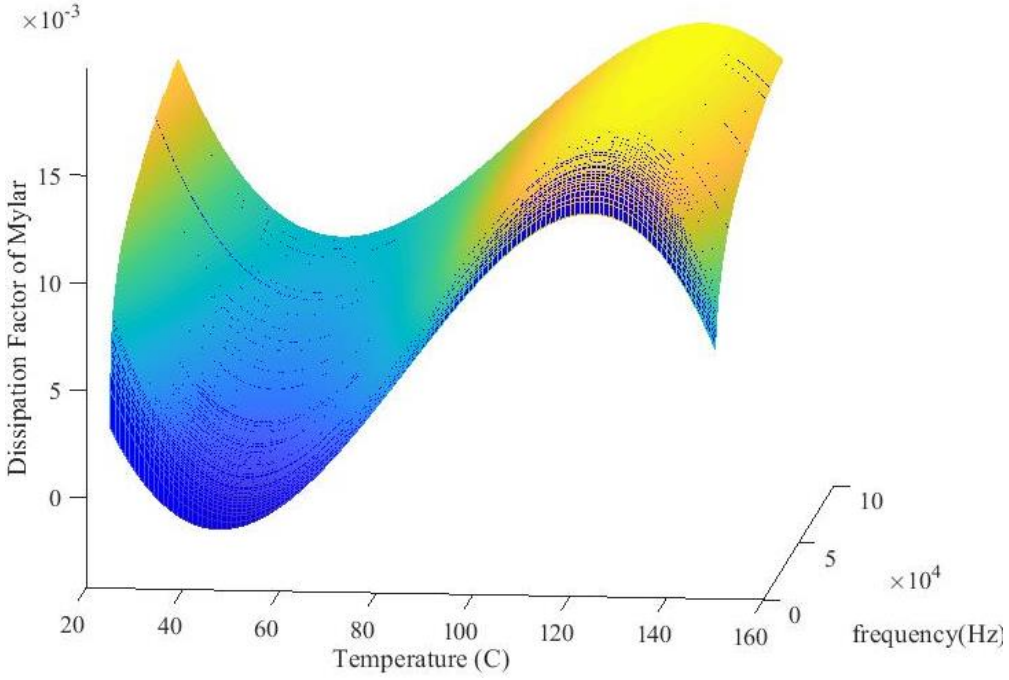

Figure 7. The dissipation factor of the Mylar vs. temperature and frequency.

4. The electric field calculation of the power cable

The electric field within the cable in the cylindrical coordinates is calculated as

$$\vec{\mathrm{E}} = E_{\mathrm{r}}\,\overrightarrow{a_r} + E_{\Phi}\,\overrightarrow{a_{\Phi}} + E_{\mathrm{z}}\,\overrightarrow{a_{\mathrm{z}}}. \tag{9}$$

The electric field components are given as

$$E_{\mathrm{r}} = -\frac{\partial V}{\partial r}, \tag{10}$$

$$E_{\Phi} = -\frac{1}{r}\frac{\partial V}{\partial \Phi}, \tag{11}$$

and

$$E_{\mathrm{z}} = -\frac{\partial V}{\partial z}. \tag{12}$$

The azimuthal component of the electric field is zero due to axisymmetry:

$$E_{\Phi} = 0. \tag{13}$$

The longitudinal component of the electric field is assumed to be zero since the cable is sufficiently long:

$$E_{\mathrm{z}} = 0. \tag{14}$$

Therefore, only the radial component of the electric field is of interest. Also, the following can be written:

$$I = \oint \vec{\mathrm{J}}\,\boldsymbol{d}\,\vec{\mathrm{S}} = \mathrm{J}2\pi\mathrm{rL}. \tag{15}$$

where J is the complex current density of the power cable within the insulator and I is the leakage current. Due to having axisymmetry, the complex leakage current density in the long power cable at the radius r can be given as

$$\vec{\mathrm{J}} = \frac{I}{2\pi\mathrm{rL}}\overrightarrow{a_r}. \tag{16}$$

In any dielectric, under the influence of an alternating voltage of angular frequency ω applied to it, active and capacitive components of the current density arise [27]. It is well-known that Cross-linked polyethylene is a non-polar dielectric with low conductivity. Remembering the relationship between the electric field and the current density in the frequency domain, the current density and the electric field within the XLPE layer are given as

$$\vec{\mathrm{J}} = j\omega\varepsilon(\omega, \mathrm{T})\,\vec{\mathrm{E}} \tag{17}$$

and

$$\vec{\mathrm{E}} = \vec{\mathrm{J}}/j\omega\varepsilon(\omega, \mathrm{T}). \tag{18}$$

Using the leakage current, the electric field within the XLPE layer can be written as

$$\mathrm{E} = \frac{I}{2\pi\mathrm{rL}j\omega\varepsilon(\omega,\mathrm{T})}. \tag{19}$$

Submitting Eq. (10) into Eq. (19), Eq. (20) is obtained:

$$-\frac{dV}{\mathrm{dr}}=\frac{I}{2\pi \mathrm{r}\mathrm{L}j\omega\varepsilon(\omega,\mathrm{T})}. \tag{20}$$

The potential difference across the XLPE layer is calculated as

$$V_{XLPE}=-\int_{r_C}^{r_{XLPE}}\frac{Idr}{2\pi \mathrm{r}\mathrm{L}j\omega\varepsilon(\omega,\mathrm{T}(\mathrm{r}))r}=-\frac{I}{2\pi Lj\omega}\int_{r_C}^{r_{XLPE}}\frac{dr}{\mathrm{r}\varepsilon(\omega,\mathrm{T}(\mathrm{r}))r} \tag{21}$$

The current density and the electric field within the Mylar layer is given as

$$\vec{\mathrm{J}}=(\sigma_{\mathrm{Mylar}}(\omega,\mathrm{T})+\mathrm{j}\omega\varepsilon_0\varepsilon_{\mathrm{Mylar}}(\omega,\mathrm{T}))\,\vec{\mathrm{E}} \tag{22}$$

and

$$\vec{\mathrm{E}}=\vec{\mathrm{J}}/(\sigma_{\mathrm{Mylar}}(\omega,\mathrm{T})+\mathrm{j}\omega\varepsilon_0\varepsilon_{\mathrm{Mylar}}(\omega,\mathrm{T})). \tag{23}$$

Using the leakage current, the electric field within the Mylar layer can be written as

$$\mathrm{E}=\frac{I}{2\pi \mathrm{r}\mathrm{L}(\sigma_{\mathrm{Mylar}}(\omega,\mathrm{T})+\mathrm{j}\omega\varepsilon_0\varepsilon_{\mathrm{Mylar}}(\omega,\mathrm{T}))}. \tag{24}$$

Submitting Eq. (10) into Eq. (24), Eq. (25) is obtained.

$$-\frac{dV}{\mathrm{dr}}=\frac{I}{2\pi \mathrm{r}\mathrm{L}(\sigma_{\mathrm{Mylar}}(\omega,\mathrm{T})+\mathrm{j}\omega\varepsilon_0\varepsilon_{\mathrm{Mylar}}(\omega,\mathrm{T}))} \tag{25}$$

The potential difference across the Mylar layer is calculated as

$$V_{Mylar}=-\int_{r_{XLPE}}^{r_{Mylar}}\frac{Idr}{2\pi \mathrm{r}\mathrm{L}(\sigma_{\mathrm{Mylar}}(\omega,\mathrm{T})+\mathrm{j}\omega\varepsilon_0\varepsilon_{\mathrm{Mylar}}(\omega,\mathrm{T}))}=-\frac{I}{2\pi L}\int_{r_{XLPE}}^{r_{Mylar}}\frac{dr}{\mathrm{r}(\sigma_{\mathrm{Mylar}}(\omega,\mathrm{T})+\mathrm{j}\omega\varepsilon_0\varepsilon_{\mathrm{Mylar}}(\omega,\mathrm{T}))}. \tag{26}$$

The potential difference across the central conductor and the shield or the XLPE and Mylar layers is found as

$$\mathrm{V}=-\int_{r_C}^{r_{Mylar}}E_{\mathrm{r}}dr=-\frac{I}{2\pi Lj\omega}\int_{r_C}^{r_{XLPE}}\frac{dr}{\mathrm{r}\varepsilon(\omega,\mathrm{T}(\mathrm{r}))r}= \tag{27}$$

$$=-\frac{I}{2\pi L}\int_{r_{XLPE}}^{r_{Mylar}}\frac{dr}{\mathrm{r}(\sigma_{\mathrm{Mylar}}(\omega,\mathrm{T})+\mathrm{j}\omega\varepsilon_0\varepsilon_{\mathrm{Mylar}}(\omega,\mathrm{T}))} \tag{28}$$

where V is the applied phase voltage in the phasor domain.

The leakage current of the power cable can be found as

$$\mathrm{I}=-\frac{2\pi LV}{\left(\frac{1}{j\omega}\int_{r_C}^{r_{Mylar}}\frac{dr}{\mathrm{r}\varepsilon(\omega,\mathrm{T}(\mathrm{r}))}+\int_{r_{XLPE}}^{r_{Mylar}}\frac{dr}{\mathrm{r}(\sigma_{\mathrm{Mylar}}(\omega,\mathrm{T})+\mathrm{j}\omega\varepsilon_0\varepsilon_{\mathrm{Mylar}}(\omega,\mathrm{T}))}\right)} \tag{29}$$

In the steady-state, the electric field within the XLPE region is calculated as

$$E_{\mathrm{XLPE}} = \frac{I}{2\pi r L j\omega \mathrm{\mathcal{E}}(\omega, T(r_C))} \tag{30}$$

By submitting Eq. (29) into Eq. (30), the electric field within the XLPE region is found as

$$E_{\mathrm{XLPE}} = -\frac{V}{\mathrm{r\mathcal{E}}\left(\int_{r_C}^{r_{XLPE}} \frac{dr}{\mathrm{r\mathcal{E}}} + j\omega \int_{r_{XLPE}}^{r_{Mylar}} \frac{dr}{\mathrm{r}(\sigma_{\mathrm{Mylar}} + \mathrm{j}\omega\mathrm{\mathcal{E}}_0\mathrm{\mathcal{E}}_{\mathrm{Mylar}})}\right)} \tag{31}$$

In the steady-state, at $r = r_C$ on the conductor, the maximum electric field within the cable occurs and is equal to

$$E_{\mathrm{XLPE}max} = \frac{I}{2\pi r_C L j\omega \mathrm{\mathcal{E}}(\omega, T(r_C))} \tag{32}$$

$$E_{\mathrm{XLPE}max} = -\frac{V}{r_C j\omega \mathrm{\mathcal{E}}(\omega, T(r_C))\left(\frac{1}{j\omega}\int_{r_C}^{r_{XLPE}} \frac{dr}{\mathrm{r\mathcal{E}}(\omega, \mathrm{T(r)})} + \int_{r_{XLPE}}^{r_{Mylar}} \frac{dr}{\mathrm{r}(\sigma_{\mathrm{Mylar}}(\omega, \mathrm{T}) + \mathrm{j}\omega\mathrm{\mathcal{E}}_0\mathrm{\mathcal{E}}_{\mathrm{Mylar}}(\omega, \mathrm{T}))}\right)} \tag{33}$$

In the steady-state, the electric field within the Mylar region is calculated as

$$E_{\mathrm{Mylar}} = \frac{I}{2\pi \mathrm{r L}(\sigma_{\mathrm{Mylar}}(\omega, \mathrm{T}) + \mathrm{j}\omega\mathrm{\mathcal{E}}_0\mathrm{\mathcal{E}}_{\mathrm{Mylar}}(\omega, \mathrm{T}))} \tag{34}$$

By submitting Eq. (29) into Eq. (34), the electric field within the XLPE region is found as

$$E_{\mathrm{Mylar}} = -\frac{j\omega V/(r(\sigma_{\mathrm{Mylar}} + \mathrm{j}\omega\mathrm{\mathcal{E}}_0\mathrm{\mathcal{E}}_{\mathrm{Mylar}}))}{\left(\int_{r_C}^{r_{XLPE}} \frac{dr}{\mathrm{r\mathcal{E}}} + j\omega \int_{r_{XLPE}}^{r_{Mylar}} \frac{dr}{\mathrm{r}(\sigma_{\mathrm{Mylar}} + \mathrm{j}\omega\mathrm{\mathcal{E}}_0\mathrm{\mathcal{E}}_{\mathrm{Mylar}})}\right)} \tag{35}$$

In the steady-state, at $r = r_{XLPE}$ on the boundary between the XLPE and the Mylar layers, the maximum electric field within the Mylar occurs and it is calculated as

$$E_{\mathrm{Mylar}max} = \frac{I}{2\pi r_{XLPE} \mathrm{L}(\sigma_{\mathrm{Mylar}}(\omega, \mathrm{T}(r_{XLPE})) + \mathrm{j}\omega\mathrm{\mathcal{E}}_0\mathrm{\mathcal{E}}_{\mathrm{Mylar}}(\omega, \mathrm{T}(r_{XLPE})))} \tag{36}$$

$$E_{\mathrm{Mylar}max} = \frac{j\omega V/(r_{XLPE}(\sigma_{\mathrm{Mylar}} + \mathrm{j}\omega\mathrm{\mathcal{E}}_0\mathrm{\mathcal{E}}_{\mathrm{Mylar}}))}{\left(\int_{r_C}^{r_{Mylar}} \frac{dr}{\mathrm{r\mathcal{E}}(\omega, \mathrm{T(r)})} + j\omega \int_{r_{XLPE}}^{r_{Mylar}} \frac{dr}{\mathrm{r}(\sigma_{\mathrm{Mylar}}(\omega, \mathrm{T}) + \mathrm{j}\omega\mathrm{\mathcal{E}}_0\mathrm{\mathcal{E}}_{\mathrm{Mylar}}(\omega, \mathrm{T}))}\right)} \tag{37}$$

5. The numerical calculation of the dielectric strength

The left integral in Eq. (31) (The XLPE layer's contribution) can be calculated numerically by taking the total number of XLPE layers as N_{XLPE}:

$$\int_{r_C}^{r_{XLPE}} \frac{dr}{\varepsilon(\omega, \mathrm{T(r)})r} \approx A_1 = \sum_{i=0}^{i=N_{XLPE}} \frac{\Delta r}{(\varepsilon_0 \varepsilon'(\omega, T(i)) - j\varepsilon_0 \varepsilon''(\omega, T(i)))r(i)} \tag{38}$$

where *i* is the XLPE layer number, $r(i) = r_C + i\Delta r$ is the radius of the i^{th}XLPE layer, and $T(i) = (T_C - T_X)\frac{\ln(r(i)/r_{XLPE})}{\ln(r_C/r_{XLPE})} + T_X$ is the temperature of the i^{th} XLPE layer.
Similarly, the right integral in Eq. (31) (The Mylar layer's contribution) can be approximated numerically by taking the total number of Mylar layers as N_{Mylar}:

$$\int_{r_{XLPE}}^{r_{Mylar}} \frac{dr}{\mathrm{r}\left(\sigma_{\mathrm{Mylar}}(\omega, \mathrm{T}) + \mathrm{j}\omega\varepsilon_0\varepsilon_{\mathrm{Mylar}}(\omega, \mathrm{T})\right)} \approx A_2$$
$$= \sum_{i=0}^{i=N_{Mylar}} \frac{\Delta r}{(\sigma_{\mathrm{Mylar}}(\omega, T(i)) + j\omega\varepsilon_{\mathrm{Mylar}}(\omega, T(i)))r(i)} \tag{39}$$

where *i* is the Mylar layer number, $r(i) = r_C + i\Delta r$ is the radius of the i^{th} Mylar layer, and $T(i) = (T_X - T_M)\frac{\ln(r(i)/r_{Mylar})}{\ln(r_{XLPE}/r_{Mylar})} + T_M$ is the temperature of the i^{th} Mylar layer.

The maximum electric field on the conductor or of the cable is found by using the sum of the Mylar and XLPE contributions:

$$E_{\mathrm{XLPE}max} \approx -\frac{V}{r_C j\omega\varepsilon\left(\omega, T(r_C)\right)\left(\frac{A_1}{j\omega} + A_2\right)} = -\frac{V}{r_C\varepsilon(\omega, T(r_C))(A_1 + j\omega A_2)} \tag{40}$$

The voltage of the cable is considered to be sinusoidal in this study. If the phase voltage is given as

$$v(t) = V_m \sin(\omega t) \tag{41}$$

The absolute value of the electric field on the conductor radius can be found calculated as

$$|E_{\mathrm{XLPE}max}| = \left|\frac{V_m}{r_C\varepsilon(\omega, T(r_C))(A_1 + j\omega A_2)}\right| \tag{42}$$

Similarly, Eq. (33) can be approximated numerically by taking the total number of Mylar layers as N_{Mylar}:

$$E_{\mathrm{Mylar}max} = \frac{j\omega V_m}{r_{XLPE}(\sigma_{\mathrm{Mylar}} + \mathrm{j}\omega\varepsilon_0\varepsilon_{\mathrm{Mylar}})\left(\frac{A_1}{j\omega} + A_2\right)} \tag{43}$$

The absolute value of the electric field within the Mylar can be found calculated as

$$\left|E_{\text{Mylar}max}\right| = \left|\frac{V_m}{r_{XLPE}(\sigma_{\text{Mylar}} + \text{j}\omega\varepsilon_0\varepsilon_{\text{Mylar}})\left(\frac{A_1}{j\omega} + A_2\right)}\right| \quad (44)$$

An m-file is written in Matlab to calculate the dielectric strength of the cable. The inputs of the Matlab file are chosen as the parameters given in Tables 1 and 2, the cable voltage amplitude, the XLPE complex permittivity function, the Mylar conductivity and permittivity functions, the conductor temperature, and the ambient temperature.

The electric fields of both the XLPE and Mylar layers are calculated for the parameters given in Tables 1-3 and are shown in Figure 8. The dielectric strength of XLPE insulator ranges from 35 to 50 kV/mm according to [24]. The electric field on the conductor is found as $2.1451.10^5$ V/m which is quite less than the dielectric strength of XLPE. The dielectric strength of Mylar insulator ranges from 1.33 to 1.66 kV/mm according to [23]. The maximum electric field at the inner radius of the Mylar layer is found as $1.195.10^5$ V/m which is less than the dielectric strength of Mylar. It has been shown in Figure 8 how the maximum electric fields of the power cable in Mylar and XLPE layers under investigation change with respect to frequency and temperature.

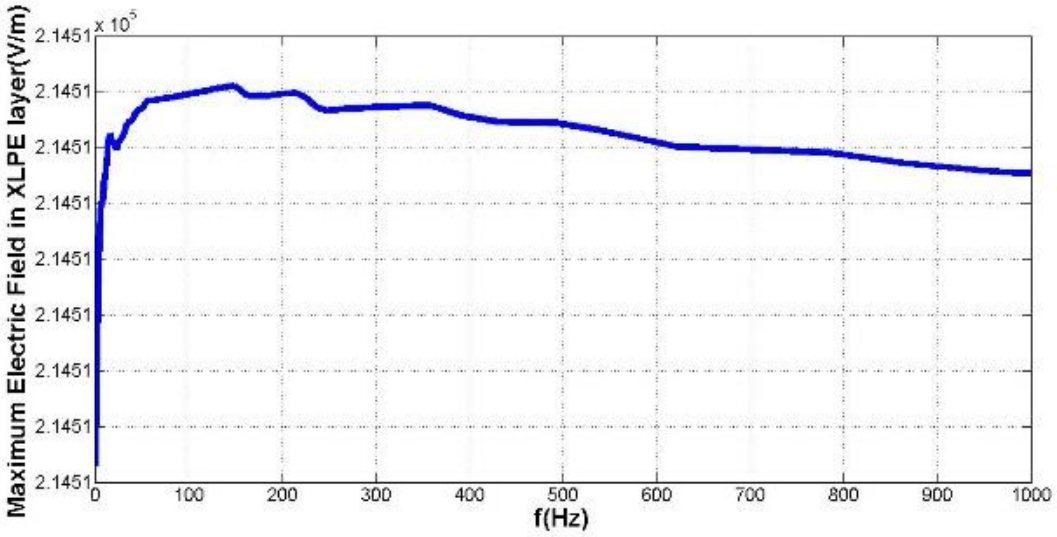

(a)

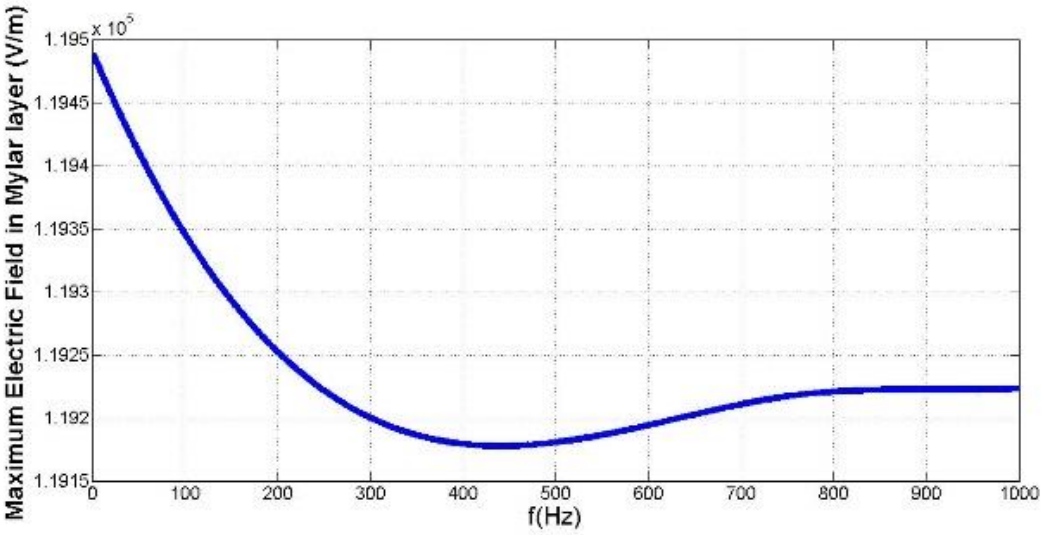

(b)

Figure 8. The maximum electric field of a) the XLPE and b) the Mylar layers vs. frequency for T_S=25 ^{0}C and T_C=90 ^{0}C.

6. Conclusion

In [15], the complex permittivity of an XLPE material is determined based on a prism-shaped sample. However, single-core cables, characterized by cylindrical shape, exhibit temperature variations dependent on the radius due to their extended length and axisymmetry. In this manuscript, the maximum electric field of such a cable is found by means of numerical integration with the XLPE and Mylar data because of the radial dependence of the cable temperature. The maximum electric field of the XLPE and Mylar layers are found considering not only the operating frequency but also the ambient and conductor temperatures. It is shown that the calculated maximum insulator electric fields remain less than the dielectric strength of the materials for the whole operation frequencies and the maximum conductor temperature considered. As a result, the model proposed in this study presents a viable approach for designing power cables, eliminating the necessity for costly programs like FEM software.

In [30], the effects of defects that may occur during the production phase of power cables on electric and magnetic field distributions are examined using the Finite Element Method Magnetics (FEMM) program. However, such a program is expensive, and it may take time to examine such a case (the electric field distribution). A simpler solution that does not need a FEM program would be quite useful. As a future work, it would be beneficial to make a similar analysis considering the defects in a similar way in cable design and go to the production stage.

Acknowledgements

This study has been supported by the research and development center of Ünika Üniversal Kablo Sanayi ve Tic. A.Ş.: Project number: **UPN-2206.**

References

[1] Moore, G.F., "Electric cables handbook", Third Edition, Blackwell Science Ltd (1997).

[2] Gouda, O.E., Matter, Z., "Effect of the temperature rise on the XLPE dielectric properties", IEEE Proceedings of the 35th Midwest Symposium on Circuits and Systems 1 (1992) : 95-98.

[3] Li, C., Chu, Z., Zhang, L., Zhang, J., Tao, J., "Insulation aging diagnosis and defect location of crosslinked polyethylene cable in the distribution network based on radio frequency identification", Materials Express 13(10) (2023) : 1772-1781.

[4] Karhan, M., Ugur, M., "XLPE İzoleli Tek Damarlı Orta Gerilim Kablolarında Elektrik Alanının Sulu Ağaçlanmaya Etkisinin İncelenmesi", Göç Sistemleri Konferansı Proceedings (2016).

[5] Karhan, M., Çakir, M., Arslan, Ö., Issi, F., Eyüpoğlu, V., "XLPE dielektrik malzemelerde elektrik alanının temas açısına ve damlacık şekline etkisi", Gazi Üniversitesi Mühendislik-Mimarlık Fakültesi Dergisi 36 (2021).

[6] Wagenaars, P., Wouters, P.A.A.F., Van der Wielen, P., Steennis, E.F., "Approximation of Transmission Line Parameters of Single-core and Three-core XLPE Cables", IEEE Transactions on Dielectrics and Electrical Insulation 17 (2010) : 106-115.

[7] Gallot-Lavallée, O., "Dielectric Materials and Electrostatics" (2013).

[8] Cooper, E., Dissado, L.A., Fothergill, J., "Application of thermoelectric aging models to polymeric insulation in cable geometry", IEEE Transactions on Dielectrics and Electrical Insulation 12 (2005) : 1-10.

[9] K.A., "Modern cable insulation", News of Electrical Engineering 2(38) (2006).

[10] Uydur, C.C., Arikan, O., Kucukaydin, B., Dursun, B., Kumru, C.F., "The Effects of Overvoltage Aging on 20 kV XLPE Power Cable", International Conference on Electrical and Electronics Engineering Proceedings (2019) : 353-357.

[11] Yu, L., "High voltage cables with cross-linked polyethylene insulation", News of Electrical Engineering 2(50) (2008).

[12] Lewis, T.J., Llewellyn, J.P., Van Der Sluijs, M.J., Freestone, J., Hampton, R.N., "Electromechanical effects in XLPE cable models", IEEE Conference on Conduction and Breakdown in Solid Dielectrics Proceedings (1995) : 269-273.

[13] Goldshtein, E., Lavrinovich, V., Slyusarenko, S., Ushakov, V., Harlov, N., Khrushchov, Y., "Problems of diagnostics of electrical power equipment to assess its residual operating lifetime", IFOST Proceedings (2007).

[14] Kovrigin, L.A., "Basics of cable technology: textbook", Perm State Technical University Publishing House (2006).

[15] Du, Y., Geng, P., Song, J., Tian, M., Pang, D., "Influence of temperature and frequency on leakage current of XLPE cable insulation", IEEE Conference Proceedings (2016) : 1-4.

[16] Liu, Y., Wang, H., Zhang, H., Du, B., "Thermal Aging Evaluation of XLPE Power Cable by Using Multidimensional Characteristic Analysis of Leakage Current", Polymers 14(15) (2022) : 3147.

[17] Szczegielniak, T., Jabłoński, P., Kusiak, D., "Analytical Approach to Current Rating of Three-Phase Power Cable with Round Conductors", Energies 16 (2023) : 1821.

[18] Aras, F., Oysu, C., "Thermal analysis of 154 kV underground cable joint using finite element method", Journal of the Faculty of Engineering and Architecture of Gazi University 22 (2007) : 281-286.
[19] Aras, F., Alekperov, V., Can, N., Kirkici, H., "Aging of 154 kV underground power cable insulation under combined thermal and electrical stresses", IEEE Electrical Insulation Magazine 23(5) (2007) : 25-33.
[20] Uydur, C., Arikan, O., "Dielectric performance analysis of laboratory aged power cable under harmonic voltages", Electrical Engineering 104 (2022).
[21] Perka, B., Piwowarski, K., "A Method for Determining the Impact of Ambient Temperature on an Electrical Cable during a Fire", Energies 14(21) (2021) : 7260.
[22] Akın, F., Arıkan, O., Uydur, C.Ç., "Analysis of solid insulating materials breakdown voltages under different voltage types", Turkish Journal of Electrical Power and Energy Systems 2(1) (2022) : 85-93.
[23] DuPont Teijin Film, S.A., "Electrical Properties of Mylar", Technical Report (2023).
[24] Nexans, "Comparison among insulation materials", Technical Documentation (2023).
[25] Boukezzi, L., Saadi, Y., Boubakeur, A., "The radial distribution of temperature in XLPE cable: An analysis with the Finite Volume Numerical Method (FVM)", Conference on Electrical Insulation and Dielectric Phenomena Proceedings (2010) : 1-4.
[26] Privezentsev, V.A., Kholodny, S.D., Ryazanov, I.B., "Basics of cable technology", Energy Publishing House (1975).
[27] Software Informer, "GetData Graph Digitizer", Software Documentation (2023).
[28] Çanta, H., Mutlu, R., Tan, R.K., "Yeni Üretilen XLPE İzolasyonlu Tek Damarlı Bir Güç Kablosunun Kaçak Empedansının Hesabı", EMO Bilimsel Dergi 14(1) (2024) : 19-26.
[29] Tan, R.K., Çanta, H., Mutlu, R., "Artificial Neural Network Models of Cross-Linked Polyethylene", Trakya Üniversitesi Mühendislik Bilimleri Dergisi 25(2) (2024) : 129-141.
[30] Uydur, C.C., Arikan, O., Kumru, O., "The Effect of Insulation Defects on Electric Field Distribution of Power Cables", IEEE International Conference on High Voltage Engineering and Application Proceedings (2018) : 1-4.